Dynamics of moment neuronal networks

Jianfeng Feng,[1,2] Yingchun Deng,[1] and Enrico Rossoni[3]
[1]*Department of Mathematics, Hunan Normal University, 410081 Changsha, People's Republic of China*
[2]*Department of Computer Science and Mathematics, Warwick University, Coventry CV4 7AL, United Kingdom*
[3]*Department of Informatics, Sussex University, Brighton BN1 9QH, United Kingdom*
(Received 2 September 2005; revised manuscript received 14 November 2005; published 7 April 2006)

A theoretical framework is developed for moment neuronal networks (MNNs). Within this framework, the behavior of the system of spiking neurons is specified in terms of the first- and second-order statistics of their interspike intervals, i.e., the mean, the variance, and the cross correlations of spike activity. Since neurons emit and receive spike trains which can be described by renewal—but generally non-Poisson—processes, we first derive a suitable diffusion-type approximation of such processes. Two approximation schemes are introduced: the usual approximation scheme (UAS) and the Ornstein-Uhlenbeck scheme. It is found that both schemes approximate well the input-output characteristics of spiking models such as the IF and the Hodgkin-Huxley models. The MNN framework is then developed according to the UAS scheme, and its predictions are tested on a few examples.

DOI: 10.1103/PhysRevE.73.041906 PACS number(s): 87.19.La, 84.35.+i

I. INTRODUCTION

During the past 20 years we have witnessed the development of the *artificial neural network* (ANN) theory and its impact on neuroscience and engineering applications. While early approaches would simply represent neurons as binary devices, most recent developments of the ANN theory have used heuristic sigmoidal-shaped input-output functions to describe the relationship between the activity of a neuron, represented by its mean firing rate, and the intensity of the synaptic input.

This picture, however, has turned out to be largely oversimplified. Indeed, it has emerged that the spike activity of a neuron is decided not only by the mean rate, but also by higher order statistics of its input [1–10]. Consider, for instance, a neuron which receives inhibitory and excitatory stochastic inputs of equal rate. Due to the fluctuations of the input, the membrane potential may occasionally cross the threshold for spiking; therefore the output firing rate will in general be positive even if the mean input is zero, thereby contradicting the basic assumptions of ANN. This simple example illustrates that the ANN theory is not much use in understanding the behavior of real nervous systems, in that it completely discards the "noisy" nature of the neural code.

The question then arises of whether it is possible to develop a framework of neural computation which includes not only the first- (mean input rate) but also the second- (fluctuations, correlations) and possibly higher-order statistics of firing. In this paper we will demonstrate that this is indeed possible, and we will lay the foundations of such a framework, which we call the *moment neuronal network* (MNN) framework.

The advantage over the ANN theory is evident. Synchronization of spiking activity, for instance, is known to play an important role for information processing in nervous systems, but it is clearly out of the scope of ANNs. For a MNN, instead, synchronized firing corresponds to the case of fully correlated activity, i.e., a correlation coefficient equal to 1. Additionally, since the MNN theory is based upon spiking neurons, all its parameters can be related to physiological observables, and its predictions can be tested directly in experiments (see next sections).

We start by investigating the activity of a single neuron. Although single-neuron models with random inputs have been widely studied in theory and numerically, most such studies are done under the assumption that the inputs are Poisson processes [11–27], which is a very rough approximation of physiological data. We will consider instead the case of *renewal process inputs*, which represent a more accurate approximation of synaptic inputs occurring *in vivo*, and becomes exact in the case of the integrate-and-fire (IF) model. The salient feature of a renewal process is that the successive occurring times of spikes are mutually independent random variables with a common distribution.

However, given the difficulties in dealing analytically with a system whose inputs are of renewal form (even in the simple Poisson case), suitable continuous approximations are required. In the literature, the so-called usual approximation scheme (UAS) was proposed earlier to approximate Poisson process inputs [17]. Also, the use of the Ornstein-Uhlenbeck (OU) process to approximate neuronal models with Poissonian inputs has been investigated for decades and most, if not all, theoretical results have been obtained for the OU approximation [28–31].

In both cases the idea is to find a diffusion process which shares the same mean and variance as the Poisson process. In Sec. II A we will extend this approach to the case of renewal process inputs and derive the corresponding UAS and OU approximating schemes. Then, in Sec. II C we will show that the first- and second-order statistics of the output spike trains generated by the IF model are not affected when the original renewal input is replaced by the continuous approximations. This result lies at the foundation of our MNN framework. Indeed, since the output spike trains of an IF neuron are again renewal processes, our approximations can be used to describe the behavior of IF neurons in a network.

 ©2006 The American Physical Society

In Sec. III we will develop the MNN framework and define the mapping between the moments of the input and the output. Similar ideas to investigate the input-output relationship of spiking neuronal networks have been investigated in the literature; see, e.g., [32]. However, as pointed out in [15] (p. 435, final paragraph), all earlier approaches were based on two key assumptions: (1) that the output of the integrate-and-fire model is again a Poisson process; (2) that the inputs are independent. The framework presented here, instead, requires neither of the assumptions. Finally, in Sec. IV we will apply the MNN framework to show how spontaneous activity can be maintained in a feedforward network, and highlight the key role played by inhibition in that context.

The MNN framework presented here can be considered as an attempt toward a general framework of computation with stochastic systems. In this respect, it would play the role of the central limit theorem in the probability theory, whereas earlier approaches based exclusively upon the mean could be likened to the law of large numbers. Besides, although the MNN theory is developed in terms of spiking neuronal networks, the learning theory developed for ANNs will be immediately applicable here. This will hopefully shed more lights on how to fill the gap between the mathematical theory of neuronal systems and neurobiology.

II. APPROXIMATIONS

A. General results

For the simplicity of notation, we first consider the case of a single renewal process. Let $T_1, T_2, \ldots$ be a series of independent and identically distributed random variables that represent the time intervals between events (spikes), and use T to denote them. Let $f(t)$ be the probability density function of T. We assume that the mean, variance, and third central moment of T exist and denote them by λ, α^2, and λ_3, respectively.

Let $\{N_t : t \geq 0\}$ be the corresponding renewal process. The expected number and variance of events in $(0,t]$ are [see Ref. [30], Eq. (4.4), Ref. [33], Eq. (1)]

$$\mu(t) \equiv \langle N_t \rangle = \frac{t}{\lambda} + \frac{\alpha^2 - \lambda^2}{2\lambda^2} + o(1) \tag{1}$$

and

$$\sigma^2(t) \equiv \langle N_t^2 \rangle - \langle N_t \rangle^2.$$

When N_t is a Poisson process, we have $\alpha^2 = \lambda^2$, $o(1) = 0$, and $\mu(t) \equiv \langle N_t \rangle = t/\lambda$. In general Eq. (1) holds true when t is large enough (see following numerical results).

A useful general result for renewal processes is that (see Ref. [33], p. 81)

$$\begin{aligned}\sigma^2(t) &= \frac{\alpha^2}{\lambda^3} t + \left(\frac{1}{6} + \frac{\alpha^4}{2\lambda^4} - \frac{\lambda_3}{3\lambda^3} \right) + o(1) \\ &= \frac{\alpha^2}{\lambda^3} \left[t + \left(\frac{\lambda^3}{6\alpha^2} + \frac{\alpha^2}{2\lambda} - \frac{\lambda_3}{3\alpha^2} \right) \right] + o(1).\end{aligned} \tag{2}$$

From Eqs. (1) and (2), we get the following theorem.

Theorem 1. The usual approximation takes the following form:

$$dN_t \sim \frac{dt}{\lambda} + \frac{\alpha}{\lambda^{3/2}} dB_t,$$

$$B_0 = \frac{\alpha^2 - \lambda^2}{2\lambda^2} \tag{3}$$

where B_t is the standard Brownian motion.

Note that in general $B_0 \neq 0$ due to the constant in Eq. (1). We call the approximation in Theorem 1 the usual approximation scheme.

Looking at the expression of the variance $\sigma^2(t)$ given by Eq. (2), we see that the leading term we omit in the UAS is $1/6 + \alpha^4/2\lambda^4 - \lambda_3/3\lambda^3$. Since in the UAS only the derivative of $\sigma^2(t)$ is used, the constant term disappears (see Ref. [16]). We therefore want to find a process $\eta^{\alpha,\lambda}(t)$ satisfying the property such that both its first- and second-order moments are in agreement with the first- and second-order moments of the renewal process. In other words, we want to find a process $\eta^{\alpha,\lambda}$ with

$$\langle [B_t - \eta^{\alpha,\lambda}(t)]^2 \rangle = t + \left(\frac{\lambda^3}{6\alpha^2} + \frac{\alpha^2}{2\lambda} - \frac{\lambda_3}{3\alpha^2} \right); \tag{4}$$

then we can approximate the renewal process $N(t)$ with the process

$$d\tilde{N}(t) \equiv \frac{1}{\lambda} dt + \frac{\alpha}{\lambda^{3/2}} d[B_t - \eta^{\alpha,\lambda}(t)].$$

We choose an Ornstein-Uhlenbeck process given by

$$d\xi(t) = -\xi(t)dt + dB_t,$$

$$\xi(0) = 0. \tag{5}$$

It is easy to show that $\xi(t) = \int_0^t \exp[-(t-s)] dB_s$. Let $\eta^{\alpha,\lambda}(t) = c\xi(t)$, where c is a constant (depending on α, λ, and λ_3) satisfying

$$\begin{aligned}\langle [B_t - \eta^{\alpha,\lambda}(t)]^2 \rangle &= t + c^2 \int_0^t \exp[-2(t-s)] ds \\ &\quad - 2c \int_0^t \exp[-(t-s)] ds \\ &= t + \frac{c^2}{2} [1 - \exp(-2t)] - 2c[1 - \exp(-t)] \\ &= t + \frac{c^2}{2} - 2c + o(1).\end{aligned} \tag{6}$$

Thus, by Eqs. (4) and (6), we have

$$c = c_r \equiv 2 + \sqrt{4 + \frac{\lambda^3}{3\alpha^2} + \frac{\alpha^2}{\lambda} - \frac{2\lambda_3}{3\alpha^2}}. \tag{7}$$

Since $\sigma^2(t) \geq 0$, letting $t \to 0$ in Eq. (2) we have $\lambda^3/6\alpha^2 + \alpha^2/2\lambda - \lambda_3/3\alpha^2 \geq 0$. Therefore

$$\Delta \equiv 4 + \frac{\lambda^3}{3\alpha^2} + \frac{\alpha^2}{\lambda} - \frac{2\lambda_3}{3\alpha^2} \geqslant 4 > 0,$$

i.e., c_r is a real and non-negative number in Eq. (7).

Hence we find an approximating scheme for $N(t)$ in terms of the OU process $\tilde{N}(t)$ defined by

$$d\tilde{N}(t) = \frac{1}{\lambda}dt + \frac{\alpha}{\lambda^{3/2}}[dB_t - c_r d\xi(t)], \tag{8}$$

where c_r is defined by Eq. (7) and $\xi(t)$ by Eq. (5).

We summarize the results above.

Theorem 2. A renewal process with the first three order statistics $\lambda, \alpha^2, \lambda_3$ of the times between spikes and the process defined by Eqs. (5), (7), and (8) share identical first- and second-order statistics, after omitting higher-order terms.

The approximation scheme defined in Theorem 2 is termed the OU scheme (OUS).

We have not seen in the literature the results of the approximation schemes presented here. One of the reasons is that the UAS is a Markov process while the original renewal process $N(t)$ usually is not a Markov process. This might be the reason that there is not a publication in the literature to explore the approximation schemes we proposed here. Of course, the OUS is not a Markov process.

B. Synaptic inputs

We consider the integrate-and-fire model with synaptic inputs. For two given quantities V_{th} (threshold) $>V_{rest}$ (resting potential), and when $V_t < V_{th}$, the membrane potential V_t satisfies the following dynamics:

$$dV_t = -L(V_t - V_{rest})dt + dI_{syn}(t),$$

$$V_0 = V_{rest} = B_0, \tag{9}$$

where $L>0$ is the decay rate, $I_{syn}(t)$ is the synaptic input given by

$$dI_{syn}(t) = a\sum_{i=1}^{p} dN_i^E(t) - b\sum_{j=1}^{q} dN_j^I(t) \tag{10}$$

where a is the magnitude of excitatory postsynaptic potentials (EPSPs), b is the magnitude of inhibitory postsynaptic potentials (IPSPs), N_i^E and N_j^I are renewal processes (EPSPs and IPSPs) generated from the ith and jth neurons, and p and q are the total number of active excitatory and inhibitory synapses. Let $T_{in,i}^E$ ($T_{in,j}^I$) be the time between events in the renewal process N_i^E (N_j^I), respectively. Once V_t is greater than V_{th}, it is reset to $V_{rest}=B_0$. We define

$$\tau =: \inf\{t > 0 : V_t = V_{th}\} \tag{11}$$

as the firing time (interspike intervals).

Since the synaptic input $I_{syn}(t)$ is modeled as a sum of renewal processes, we can apply here the results derived in the previous section. For the simplicity of notation, we assume that for $i=1,2,\ldots,p$, $j=1,2,\ldots,q$

$$T_{in,i}^E = T_{in,j}^I = T$$

where the mean, variance, and third central moment of T are given by λ, α^2, and λ_3, respectively. Let us further suppose that

$$p = q,$$

$$b = ar, \quad r \geqslant 0. \tag{12}$$

Here r is the ratio between inhibitory and excitatory inputs. When $r=0$, all inputs are excitatory; when $r=1$, inhibitory inputs equal excitatory inputs.

Therefore, according to Eq. (8), we have

$$dN_i^E(t) \sim \frac{1}{\lambda}dt + \frac{\alpha}{\lambda^{3/2}}[dB_i^E(t) - c_r d\xi_i^E(t)], \tag{13}$$

where $\xi_i^E(t) = \int_0^t \exp[-(t-s)]dB_i^E(s)$ and $B_i^E(t)$ is the standard Brownian motion.

Now we let $d\xi^{E,p}(t) \equiv \sum_{i=1}^{p} d\xi_i^E(t)$; then by Eq. (5), $\xi^{E,p}(t)$ satisfies

$$d\xi^{E,p}(t) = -\xi^{E,p}(t)dt + \sqrt{p}dB^E(t),$$

$$\xi^{E,p}(0) = 0.$$

Hence, by Eq. (13) and the equation above

$$\sum_{i=1}^{p} dN_i^E(t) \sim \frac{p}{\lambda}dt + \sqrt{p}\frac{\alpha}{\lambda^{3/2}}dB^E(t) - \frac{\alpha c_r}{\lambda^{3/2}}d\xi^{E,p}(t),$$

where $\xi^{E,p}(t) = \sqrt{p}\int_0^t \exp[-(t-s)]dB^E(s)$, and $B^E(t)$ is again the standard Brownian motion.

A similar result holds for $\sum_{j=1}^{q} dN_j^I(t)$. Hence, by Eqs. (10) and (12), we have

$$dI_{syn}(t) \approx \frac{ap(1-r)}{\lambda}dt + \frac{a\alpha}{\lambda^{3/2}}[\sqrt{p(1+r^2)}dB_t - c_r d\xi^{p,r}(t)] \tag{14}$$

and

$$dV_t = -L(V_t - V_{rest})dt + \frac{ap(1-r)}{\lambda}dt + \frac{a\alpha}{\lambda^{3/2}}[\sqrt{p(1+r^2)}dB_t - c_r d\xi^{p,r}(t)] \tag{15}$$

where B_t is the standard Brownian motion and $\xi^{p,r}$ is the OU process satisfying

$$d\xi^{p,r}(t) = -\xi^{p,r}(t)dt + \sqrt{p(1+r^2)}dB_s,$$

$$\xi^{p,r}(0) = 0,$$

i.e., $\xi^{p,r}(t) = \sqrt{p(1+r^2)}\int_0^t \exp[-(t-s)]dB_s$.

In summary, we have proposed two approximation schemes: (1) the UAS (by Theorem 1)

$$dv_t = -L(v_t - V_{rest})dt + \frac{ap(1-r)}{\lambda}dt + \frac{a\alpha}{\lambda^{3/2}}\sqrt{p(1+r^2)}dB_t,$$

$$v_0 = V_{rest} = B_0, \tag{16}$$

and (2) the OUS (by Theorem 2)

$$\begin{aligned} dV_t &= -L(V_t - V_{rest})dt + \frac{ap(1-r)}{\lambda}dt \\ &\quad + \frac{a\alpha}{\lambda^{3/2}}[\sqrt{p(1+r^2)}dB_t - c_r d\xi^{p,r}(t)], \\ d\xi^{p,r}(t) &= -\xi^{p,r}(t)dt + \sqrt{p(1+r^2)}dB_s, \\ V_0 &= V_{rest} = B_0, \\ \xi^{p,r}(0) &= 0, \end{aligned} \tag{17}$$

where

$$c_r = 2 - \sqrt{4 + \frac{\lambda^3}{3\alpha^2} + \frac{\alpha^2}{\lambda} - \frac{2\lambda_3}{3\alpha^2}}.$$

As we mentioned before, the interest of the UAS lies in the fact that all similar results in the literature are exclusively developed for Poisson processes. In the next section we will carry out a detailed numerical comparison between the statistics of the output spike trains obtained with the two schemes above and with the original renewal process.

C. Neuronal model with Gamma-distributed inputs: IF model

1. Theoretical results

In order to carry out numerical simulations, we further assume that T is distributed according to a Gamma distribution[1] with positive parameters κ, μ, i.e., the corresponding density function is

$$f(t) = \left(\frac{1}{\mu}\right)^{\kappa} \frac{t^{\kappa-1}e^{-t/\mu}}{\Gamma(\kappa)}. \tag{18}$$

Therefore we have $\langle T\rangle = \kappa\mu$, $\mathrm{var}(T) = \kappa\mu^2$, and the third central moment

$$\begin{aligned} \langle (T-\kappa\mu)^3\rangle &= \langle T^3\rangle - 3\kappa\mu\langle T^2\rangle + 3\kappa^2\mu^2\langle T\rangle - \kappa^3\mu^3 \\ &= \frac{\mu^3\Gamma(\kappa+3)}{\Gamma(\kappa)} - 3(\kappa\mu^2 + \kappa^2\mu^2)\kappa\mu + 2\kappa^3\mu^3 \\ &= \mu^3(\kappa+2)(\kappa+1)\kappa - 3\kappa^2\mu^3 - \kappa^3\mu^3 \\ &= 2\kappa\mu^3, \end{aligned}$$

that is,

$$\lambda = \kappa\mu,$$

$$\alpha^2 = \kappa\mu^2,$$

$$\lambda_3 = 2\kappa\mu^3.$$

Therefore, in the UAS, Eq. (9) becomes

$$\begin{aligned} dv_t &= -L(v_t - V_{rest})dt + \frac{ap(1-r)}{\kappa\mu}dt + \frac{a}{\sqrt{\kappa^2\mu}}\sqrt{p(1+r^2)}dB_t, \\ v_0 &= V_{rest} = B_0, \end{aligned} \tag{19}$$

while, in the OU approximation, we get the system

$$\begin{aligned} dV_t &= -L(V_t - V_{rest})dt + \frac{ap(1-r)}{\kappa\mu}dt \\ &\quad + \frac{a}{\sqrt{\kappa^2\mu}}[\sqrt{p(1+r^2)}dB_t - c_g d\xi^{p,r}(t)], \\ d\xi^{p,r}(t) &= -\xi^{p,r}(t)dt + \sqrt{p(1+r^2)}dB_s, \\ V_0 &= V_{rest} = B_0, \\ \xi^{p,r}(0) &= 0, \end{aligned} \tag{20}$$

where $c_g = 2 - \sqrt{4 + \kappa^2\mu/3 - \mu/3}$, and $\kappa > \max\{0, 1 - 12/\mu\}$.

2. Numerical results I

For our numerical simulations we used the parameters: $a = 0.5$ mV, $b = ar$, $V_{rest} = B_0$, $V_{th} = 20$ mV, $p = q = 100$, $\gamma = 20$ ms. The same parameters have been employed elsewhere [16], and are thought to be in the physiological range for visual cortex cells. The membrane equations Eqs. (9), (19), and (20) were solved numerically using a step size of 0.01 ms, with $I_{syn}(0) = 0$. After each spike, V_t was reset to $V_{rest} = B_0$, while $I_{syn}(t)$ was left unchanged.

We considered different values of the parameters κ and μ for the Gamma distribution of the time T between synaptic inputs. Also, we vary the ratio r between inhibitory and excitatory inputs in the range where the model displayed spiking activity. For each choice of κ, μ, and r, we generated 1000 spikes, then calculated the mean output firing rate $\langle\tau\rangle^{-1}$ [see Eq. (11)] and the coefficient of variation (CV) of the interspike intervals, $C_{var} = \sqrt{\mathrm{var}(\tau)}/\langle\tau\rangle^2$. In the following we will refer to the latter as the "output CV."

Figure 1 (top) shows the results obtained with $\kappa = 0.5$, $\mu = 10$ (i.e., $\langle T\rangle = 5$ ms). In this case, the output CV obtained with renewal process inputs is smaller than in the UAS and the OUS approximations. Figure 1 (middle) corresponds to $\kappa = 1$, $\mu = 10$ ($\langle T\rangle = 10$ ms), i.e., a Poissonian input. In this case, the UAS and OUS approximations gave identical results. Figure 1 (bottom) shows the results obtained with $\kappa = 5$, $\mu = 2$ ($\langle T\rangle = 10$ ms).

3. Numerical results II

Here we consider the IF model with spike trains generated by an IF model as inputs to a further IF model.

First, we simulated an IF model with Poisson inputs of intensity $\lambda = 0.2, 0.1$ (i.e., 100 and 200 Hz) and $r = 0.6$, and generated 200 spike trains with interspike intervals $T^E_{in,i}, T^I_{in,j}$, $i = 1, 2, \ldots, p$, $j = 1, 2, \ldots, q$. These were sent as inputs to another IF model. To carry out a comparison of various models, we used 5000 spikes to calculate the mean and variance in the following equations:

[1] Of course, it is easy to generalize the following results to other distributions, e.g., the inverse Gaussian distribution [16].

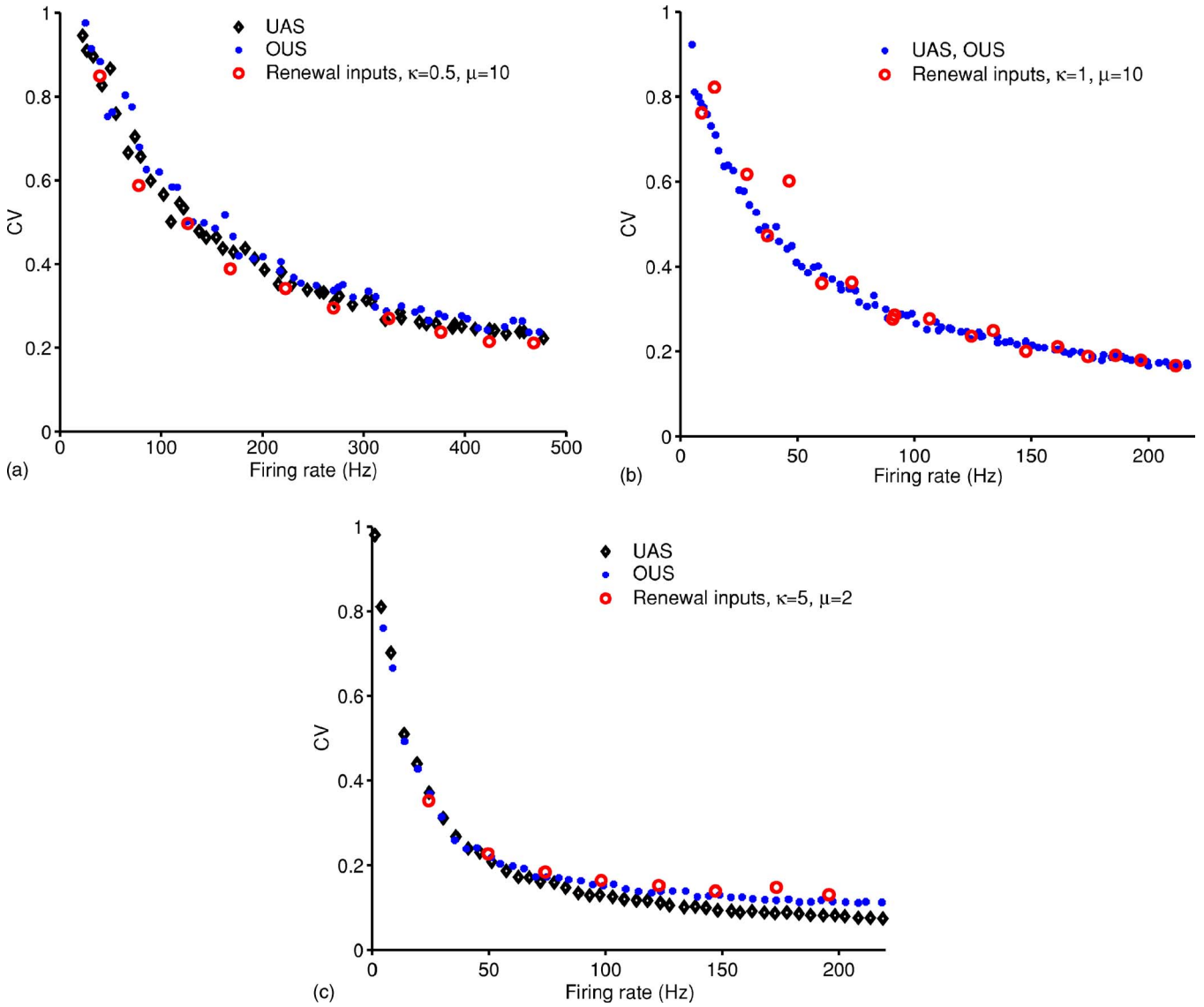

FIG. 1. (Color online) The coefficient of variation (CV) of the output interspike intervals plotted vs the output firing rate for an IF model with renewal process inputs [(red) empty circles, parameters of the Gamma distribution as indicated], and corresponding UAS [(black) diamonds] and OUS [(blue) circles] continuous approximations. Different data points correspond to varying the inhibitory-excitatory ratio.

$$\kappa\mu = \langle T^E_{in,i} \rangle,$$

$$\kappa\mu^2 = \mathrm{var}(T^E_{in,i}).$$

By solving them we obtain $\kappa=10.7509$, $\mu=0.5425$ for $\lambda=0.2$, and $\kappa=8.3642$, $\mu=1.6301$ for $\lambda=0.1$.

Using these parameters, we approximated the input as described in the previous subsection. Finally, 500 output spikes were generated with $r=0,0.05,\ldots,0.8$ and the corresponding output mean firing rate and CV were calculated, as shown in Fig. 2.

In Fig. 2 (top) we plotted the interspike interval distributions of the natural inputs obtained for $\lambda=0.2$ (left) and 0.1 (right). It is clearly seen that such distributions cannot be fitted by exponentials, that is natural inputs cannot be simply approximated by Poisson process. Figure 2 (bottom) shows the output firing rate and CV obtained in response to natural inputs and their UAS and OUS approximations. We conclude that both schemes work reasonably well, with the OUS outperforming the UAS, especially at high frequencies.

D. Neuronal model with Gamma-distributed inputs: Biophysical models

We apply here the results of the previous section to the case of a biophysical neuronal model with renewal inputs. In particular, we consider the Hodgkin-Huxley (HH) model with parameters given as in the literature [34,35]:

$$C\,dV = -g_{\mathrm{Na}}m^3h(V-V_{\mathrm{Na}})dt - g_k n^4(V-V_k)dt - g_L(V-V_L)dt + dI_{syn}(t) \tag{21}$$

where $I_{syn}(t)$ is defined by Eq. (10) and

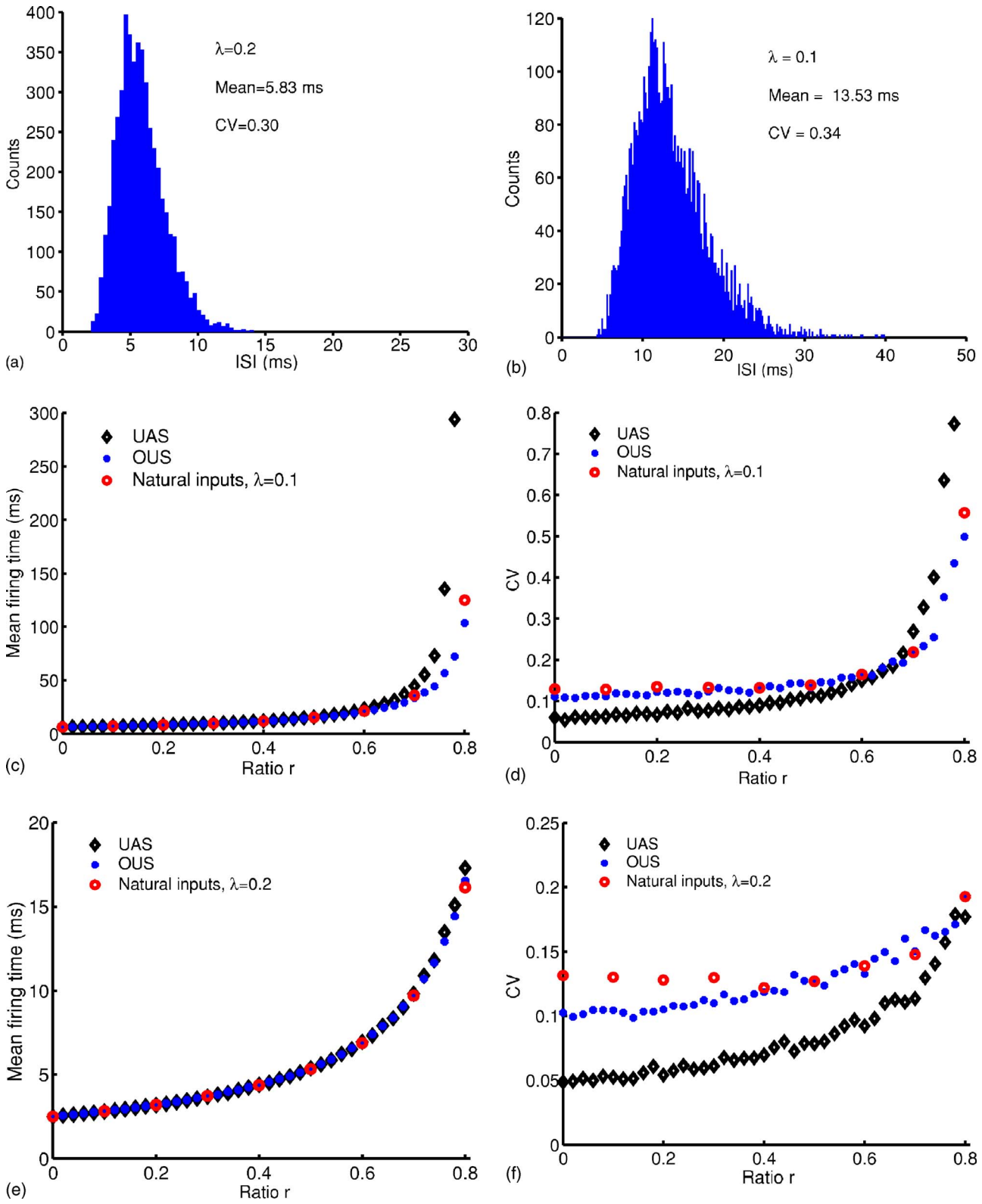

FIG. 2. (Color online) (Top) The interspike interval distributions of natural inputs obtained with Poisson intensity $\lambda=0.2$ (left), 0.1 (right); histograms were constructed over 5000 intervals, bin size 0.2 ms. (Middle, bottom) The mean (left) and the coefficient of variation (CV, right) of the interspike intervals generated by the IF model with natural inputs [(red) empty circles], and by the corresponding UAS [(black) diamonds] and OUS approximating schemes [(blue) circles], plotted vs the inhibitory-excitatory ratio r.

$$\frac{dn}{dt} = \frac{n_\infty - n}{\tau_n}, \quad \frac{dm}{dt} = \frac{m_\infty - m}{\tau_m}, \quad \frac{dh}{dt} = \frac{h_\infty - h}{\tau_h},$$

and

$$n_\infty = \frac{\alpha_n}{\alpha_n + \beta_n}, \quad m_\infty = \frac{\alpha_m}{\alpha_m + \beta_m}, \quad h_\infty = \frac{\alpha_h}{\alpha_h + \beta_h},$$

$$\tau_n = \frac{1}{\alpha_n + \beta_n}, \quad \tau_m = \frac{1}{\alpha_m + \beta_m}, \quad \tau_h = \frac{1}{\alpha_h + \beta_h},$$

with

$$\alpha_n = \frac{0.01(V+55)}{1 - \exp\left(-\frac{V+55}{10}\right)}, \quad \beta_n = 0.125 \exp\left(-\frac{V+65}{80}\right),$$

$$\alpha_m = \frac{0.1(V+40)}{1 - \exp\left(-\frac{V+40}{10}\right)}, \quad \beta_m = 4 \exp\left(-\frac{V+65}{18}\right),$$

$$\alpha_h = 0.07 \exp\left(-\frac{V+65}{20}\right), \quad \beta_h = \frac{1}{1 + \exp\left(-\frac{V+35}{10}\right)}.$$

The parameters used in Eq. (21) are $C=1\ \mu\text{F/cm}^2$, $g_{\text{Na}}=120\ \text{mS/cm}^2$, $g_k=36\ \text{mS/cm}^2$, $g_L=0.3\ \text{mS/cm}^2$, $V_k=-77$ mV, $V_{\text{Na}}=50$ mV, and $V_L=-54.4$ mV. All the parameters used for the synaptic inputs are the same as in the previous sections. The initial values for m, n, h, I_{syn}, and V are 0.06, 0.35, 0.6, B_0, and −65 mV, respectively.

In Fig. 3 we report the mean and CV of the firing time vs the ratio r, as obtained for different values of the input parameters: $\kappa=0.5, \mu=10, a=0.5$ (upper panel); $\kappa=1, \mu=10$, $a=0.5$ (Poisson input case, middle panel); and $\kappa=10$, $\mu=2, a=1$ (bottom panel). It appears that for $\kappa<1$ the UAS provides a better approximation than the OUS. However, for $\kappa>1$, only the OUS was applicable. For example, when $\kappa=10$, the HH model could not generate a spike even when the inhibitory-excitatory ratio was reduced down to $r=0.2$. The reason is that the HH model is particularly sensitive to the second-order statistics of the input, which is not fully included in the UAS. This result confirms that the OUS is more effective in approximating the effect of non-Poissonian inputs.

III. MOMENT MAPPING

From the results of the previous section, we have that both the UAS and the OUS work well for the IF model within a range of physiologically realistic firing rates, say up to 150 Hz. Therefore, we are in the position to develop our MNN framework.

We confine our discussion to feedforward networks, although the results presented below can be easily generalized to feedback and recurrent networks.

In comparison with the previous sections, a slightly more complicated notation is needed here. For $V_{th}>V_{rest}$ and when $v_i^{(k+1)}(t)<V_{th}$, the membrane potential of the ith neuron in the $(k+1)$th layer $v_i^{(k+1)}(t)$ satisfies the following dynamics:

$$dv_i^{(k+1)}(t) = -L[v_i^{(k+1)}(t) - V_{rest}]dt + dI_{i,syn}^{(k+1)}(t),$$

$$v_i^{(k+1)}(0) = V_{rest}, \tag{22}$$

where the synaptic input $I_{i,syn}^{(k+1)}(t)$ is given by

$$dI_{i,syn}^{(k+1)}(t) = \sum_{j=1}^{p^{(k)}} w_{ij}^{E,(k)} dN_j^{E,(k)}(t) - \sum_{j=1}^{q^{(k)}} w_{ij}^{I,(k)} dN_j^{I,(k)}(t). \tag{23}$$

Here $w_{ij}^{E,(k)}$ is the magnitude of EPSPs, $w_{ij}^{I,(k)}$ is the magnitude of IPSPs, $N_i^{E,(k)}$ and $N_j^{I,(k)}$ are renewal processes (EPSPs and IPSPs) generated from neurons i and j with interspike intervals and $T_{jm}^{I,(k)}$, $m=1,2,\ldots$, and $p^{(k)}$ and $q^{(k)}$ are the total number of active excitatory and inhibitory neurons in the kth layer. Once $v_i^{(k+1)}(t)$ is greater than or equal to V_{th}, it is reset to V_{rest}.

According to Eq. (1), we have

$$\frac{dN_i^{E,(k)}(t)}{dt} \to N\left(\frac{1}{\langle T_{ij}^{E,(k)}\rangle}, \frac{[\langle (T_{ij}^{E,(k)})^2\rangle - \langle T_{ij}^{E,(k)}\rangle^2]}{\langle T_{ij}^{E,(k)}\rangle^3}\right)$$

where $N(\cdot,\cdot)$ is the normal distribution. A more accurate approximation can be obtained using a similar idea as employed in Theorem 2, although the moment mapping becomes very complicated in this case. Besides, our previous results suggest that, for the IF model, the UAS is already a good approximation in most cases.

We introduce more notation by defining

$$\mu_{ij}^{E,(k)} = \frac{1}{\langle T_{ij}^{E,(k)}\rangle + T_{ref}}, \quad (\sigma_{ij}^{E,(k)})^2 = \frac{[\langle (T_{ij}^{E,(k)})^2\rangle - \langle T_{ij}^{E,(k)}\rangle^2]}{\langle T_{ij}^{E,(k)}\rangle^3}$$

where T_{ref} is the refractory period (5 ms in all simulations below). For the ith neuron in the kth layer, we have (by Theorem 1)

$$dN_i^{E,(k)}(t) \sim \mu_{i1}^{E,(k)} dt + \sigma_{i1}^{E,(k)} dB_i^{E,(k)}(t) \tag{24}$$

where $B_i^{E,(k)}(t)$ is the standard Brownian motion with a correlation coefficient $\rho_{ij}^{(k)}, i, j=1,\ldots,N^{(k)}$. Summarizing the results above, we obtain

$$\sum_{j=1}^{p^{(k)}} w_{ij}^{E,(k)} dN_j^{E,(k)}(t) = \sum_j w_{ij}^{E,(k)} \mu_{j1}^{E,(k)} dt + \sum_j w_{ij}^{E,(k)} \sigma_{j1}^{E,(k)} dB_j^{E,(k)}(t).$$

Let us further suppose that $p^{(k)}=q^{(k)}$ and, for simplicity of notation,

$$\mu_j^{(k)} = \mu_{j1}^{E,(k)} = \mu_{j1}^{I,(k)},$$

$$\sigma_j^{(k)} = \sigma_{j1}^{E,(k)} = \sigma_{j1}^{I,(k)},$$

$$rw_{ij}^{(k)} = rw_{ij}^{E,(k)} = w_{ij}^{I,(k)}, \tag{25}$$

where $i=1,\ldots,p^{(k+1)}$, $j=1,\ldots,p^{(k)}$, and r is the ratio between inhibitory inputs and excitatory inputs. In particular,

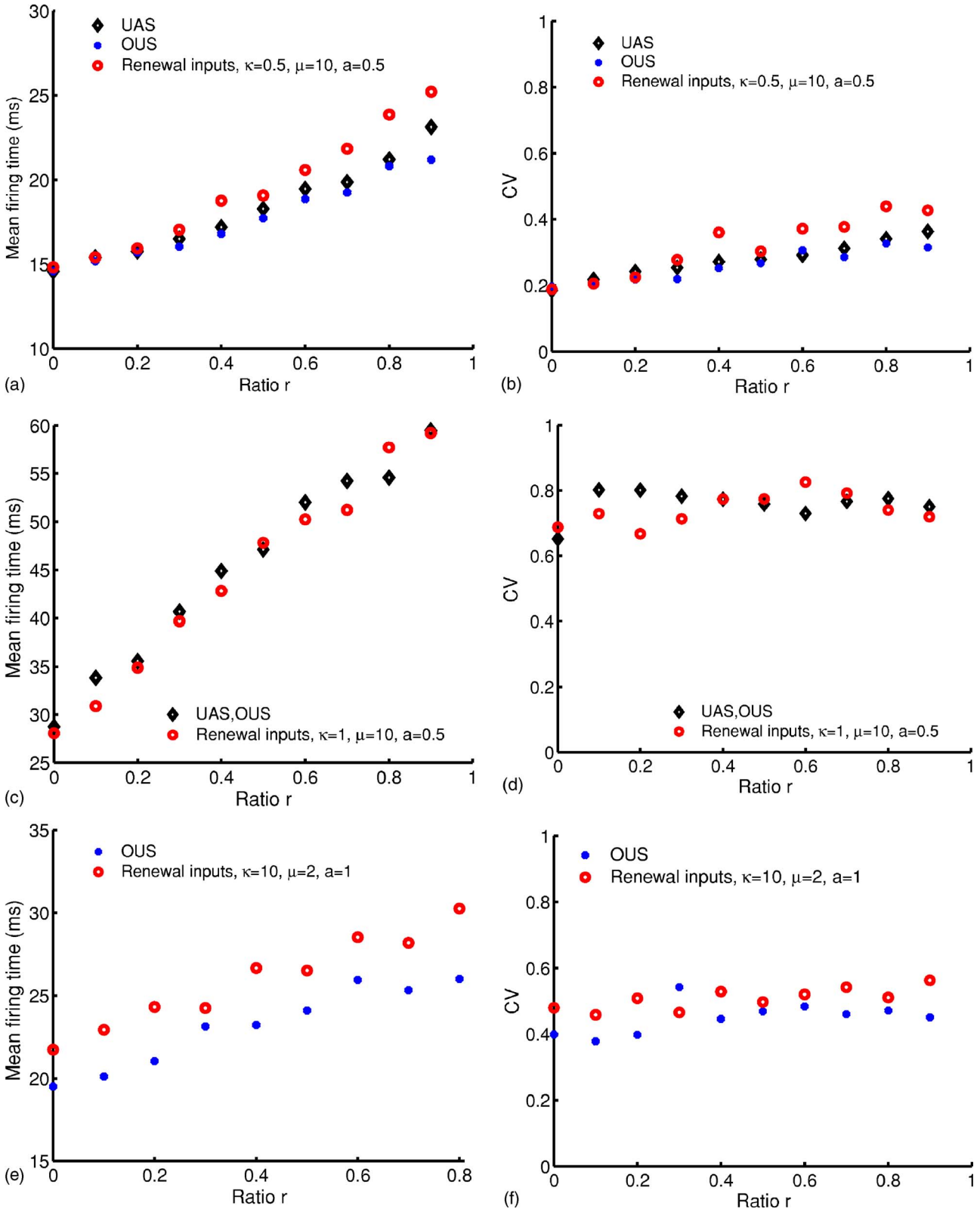

FIG. 3. (Color online) The mean (left) and the coefficient of variation (CV, right) of the interspike intervals generated by the HH model with renewal process inputs, and by the corresponding UAS [(black) diamonds] and OUS [(blue) circles] approximations (where applicable), are plotted vs the inhibitory-excitatory input ratio r. Reported on the legend are the values of the parameters κ, μ used for the Gamma distribution, and the post-synaptic potentials' amplitude a (in mV).

when $r=0$ the neuron receives exclusively excitatory inputs; when $r=1$ the inhibitory and excitatory inputs are exactly balanced. Now we have

$$dI_{i,syn}^{(k+1)} = \sum_j w_{ij}^{(k)} \mu_j^{(k)} (1-r)dt + \sum_j w_{ij}^{(k)} \sigma_j^{(k)} \sqrt{1+r^2} dB_j^{(k)}(t) \tag{26}$$

where $B_i^{(k)}(t),\ i=1,\ldots,p^{(k)}$ are correlated Brownian motions with correlation coefficient $\rho_{ij}^{(k)}$.

In the following we define $\tau_{i0}^{(k)}=0$ and

$$\tau_{ij}^{(k+1)} = \inf\{t: v_i^{(k+1)}(t) \geqslant V_{th}, t > \tau_{i(j-1)}^{(k+1)}\}, \quad j=1,2,\ldots.$$

Then

$$T_{ij}^{(k+1)} = \tau_{ij}^{(k+1)} - \tau_{ij-1}^{(k+1)}, \quad j=1,2,\ldots. \tag{27}$$

Let $T_i^{(k+1)}=T_{i1}^{(k+1)}$ be the interspike intervals of renewal processes $N_i^{E,(k+1)}$ and $N_i^{I,(k+1)}$. In terms of Siegert's expression [15] we have the expression of all moments of the output interspike interval distribution. In particular, for the mean we have

$$\langle T_i^{(k+1)} \rangle = \frac{2}{L} \int_{A_i^{(k)}(0)}^{A_i^{(k)}(V_{th})} g(x)dx, \quad A_i^{(k)}(y) = \frac{yL - \bar{\mu}_i^{(k)}}{\bar{\sigma}_i^{(k)} \sqrt{L}}, \tag{28}$$

where

$$\bar{\mu}_i^{(k)} = \sum_j w_{ij}^{(k)} \mu_j^{(k)} (1-r),$$

$$(\bar{\sigma}_i^{(k)})^2 = \sum_{m,n} w_{im}^{(k)} \sigma_m^{(k)} w_{in}^{(k)} \sigma_n^{(k)} \rho_{mn}^{(k)} (1+r^2), \tag{29}$$

and

$$g(x) = \exp(x^2) \int_{-\infty}^{x} \exp(-u^2)du,$$

while for the variance we have

$$\mathrm{var}(T_i^{(k+1)}) = \frac{4}{L^2} \int_{A_i^{(k)}(0)}^{A_i^{(k)}(V_{th})} \exp(x^2) \left(\int_{-\infty}^{x} \exp(-u^2) g^2(u)du \right) dx. \tag{30}$$

To complete the description of the moment mapping (see below for definition) we need to consider the relationship between the input and the output correlations. Unfortunately, such a relationship is difficult to derive analytically, so we had to resort to numerical simulations. To this end, we simulated two IF neurons with inputs given by

$$\mu(1-r)dt + \sqrt{\mu(1+r^2)} dB^{(i)}, \quad i=1,2,$$

where μ is a constant and $B^{(i)}$ are correlated Brownian motions with correlation coefficient ρ_{in}. In Fig. 4 we have plotted the output correlation coefficient ρ_{out} defined as a function of the input correlation for various values of the ratio r. The results indicate that the input-output relationship is close to the identity, independently of r and μ.

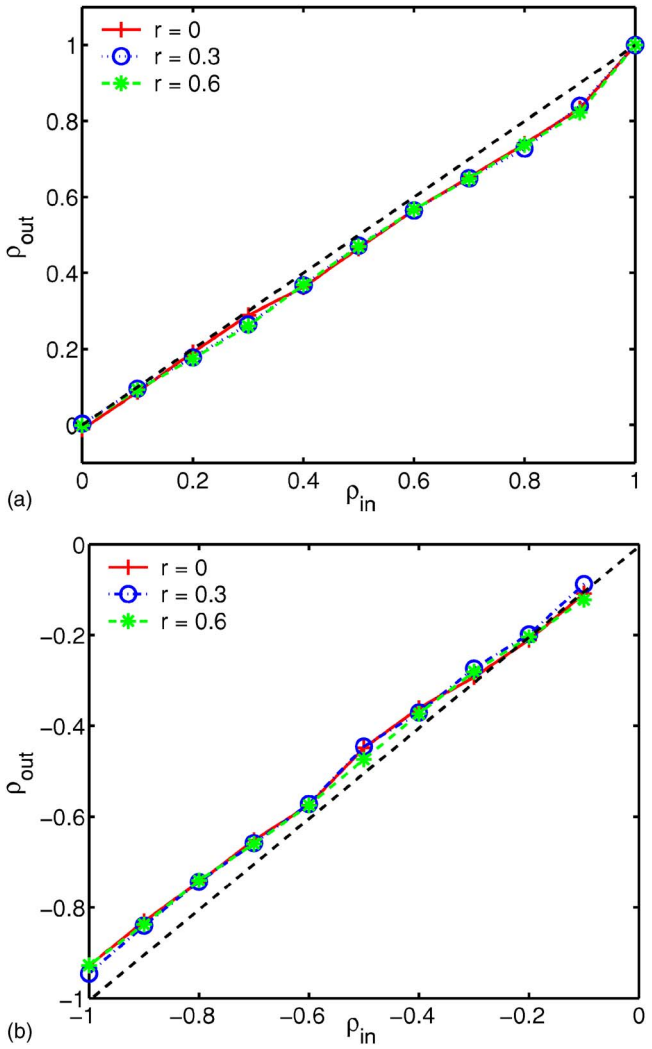

FIG. 4. (Color online) The relationship between the input and output correlation coefficients (ρ_{in}, ρ_{out}) for an IF model with Gaussian input. The output correlation coefficient was calculated over a series of 5000 spikes for each value of r. The calculated relationship is almost linear and independent of the ratio r for both positive (top) and negative (bottom) input correlation.

Hence, we can assume that the following *heuristic* relationship holds:

$$\rho_{ij}^{(k+1)} = \frac{\sum_{m,n} w_{im}^{(k)} \sigma_m^{(k)} w_{jn}^{(k)} \sigma_n^{(k)} \rho_{mn}^{(k)}}{\sqrt{\sum_{m,n} w_{im}^{(k)} \sigma_m^{(k)} w_{in}^{(k)} \sigma_n^{(k)} \rho_{mn}^{(k)}} \sqrt{\sum_{m,n} w_{jm}^{(k)} \sigma_m^{(k)} w_{jn}^{(k)} \sigma_n^{(k)} \rho_{mn}^{(k)}}}. \tag{31}$$

Note that the right-hand side of Eq. (31) is the correlation of the inputs to the ith and the jth neurons in the $(k+1)$th layer.

Let us have a few words on the implications of Eq. (31). Assume that $w_{im}^{(k)}=w>0$, $\sigma_m^{(k)}=\sigma>0$, and $\rho_{mn}^{(k)}=\rho, m\neq n$, then we have

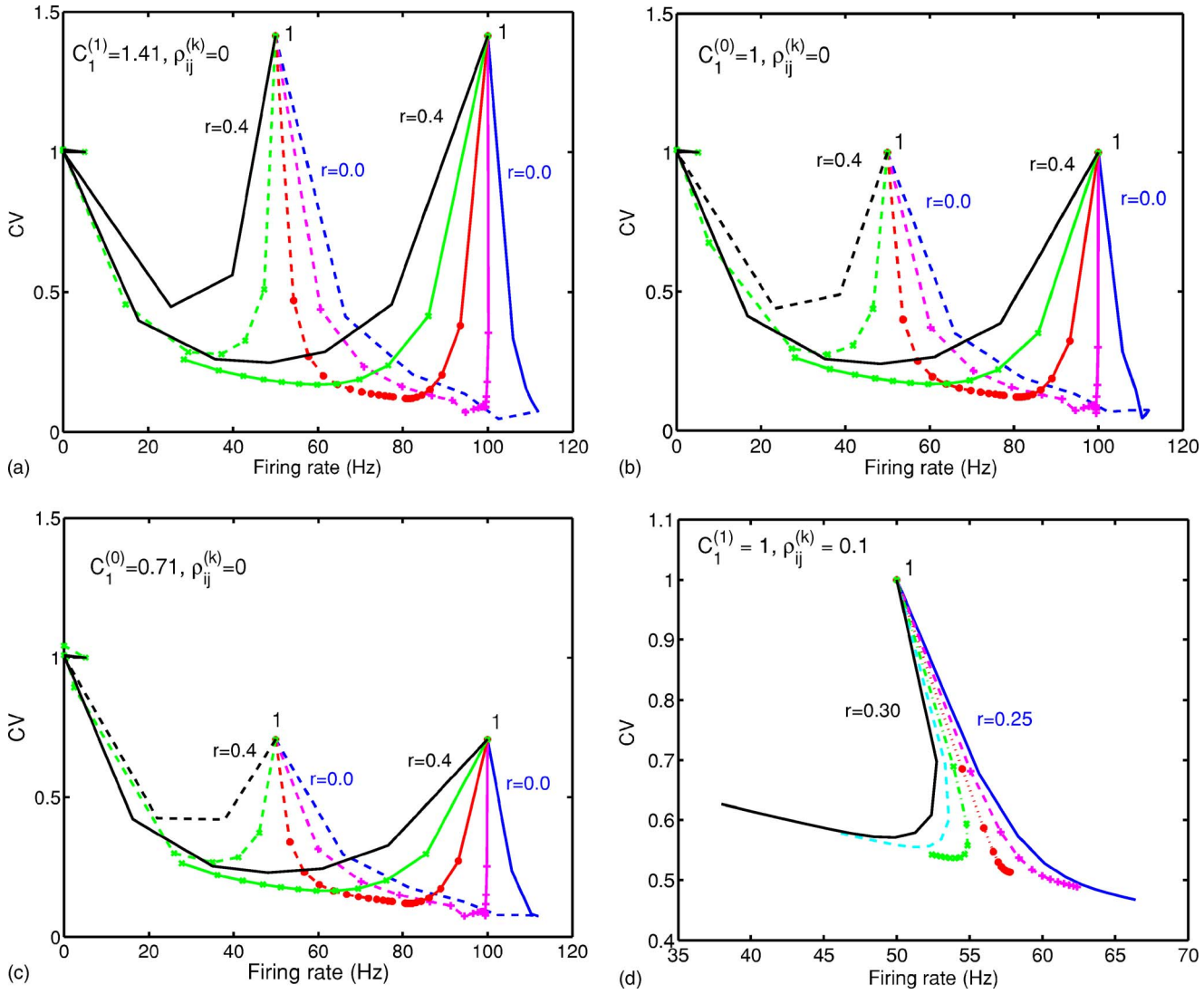

FIG. 5. (Color online) Propagation of activity in a homogeneous feedforward MNN. For each layer k, the output firing rate ($\mu_1^{(k)}$) and the coefficient of variation (CV) of the interspike intervals ($C_1^{(k)}$) are reported on the abscissa and the ordinate, respectively. Points labeled 1 correspond to the first layer; points corresponding to successive layers are connected by lines. Results were obtained for $p^{(k)}=100$, $\rho_{ij}=0$, $\mu_1^{(1)}=100$ Hz (solid lines), 50 Hz (dashed lines), and $C_1^{(1)}=\sqrt{2}$ (top left), 1 (top right), and $\sqrt{0.5}$ (bottom left). (Bottom right) Results obtained for $r=0.25,0.26,\ldots,0.3$, $\rho_{ij}^{(k)}=0.1, C_i^{(1)}=1, \mu_i^{(1)}=50$ Hz.

$$\rho_{ij}^{(k+1)} = \frac{p^{(k)} + p^{(k)}(p^{(k)}-1)\rho}{p^{(k)} + p^{(k)}(p^{(k)}-1)\rho} = 1,$$

where $p^{(k)}$ is the total number of neurons in the kth layer. In other words, the neuronal activity is fully correlated (synchronized). Similar synchronized spike trains have been observed earlier in the literature [17] (see Fig. 7 there) for feedforward spiking networks. In the general case where $w_{ij}^{(k)}$, $\sigma_m^{(k)}$, and $\rho_{ij}^{(k)}$ are not homogeneous, and the relationship between the input and the output correlations differs from the identity, $\rho_{ij}^{(k+1)}$ will be different from 1.

Another extremal case is observed when the vectors $w_i^{(k)}=\{w_{im}^{(k)}, m=1,\ldots,p^{(k)}\}$ and $w_j^{(k)}=\{w_{jm}^{(k)}, m=1,\ldots,p^{(k)}\}$ are orthogonal. Since we require that $w_{im}^{(k)} \geqslant 0$, we conclude that $\Sigma_{m,n} w_{im}^{(k)} \sigma_m^{(k)} w_{jn}^{(k)} \sigma_n^{(k)} \rho_{mn}^{(k)} = 0$ and therefore $\rho_{ij}^{(k+1)}=0$. Assuming that $A, B \subset \{1,\ldots,p^{(k+1)}\}$, $A \cap B = \varnothing$, and $w_i^{(k)} \perp w_j^{(k)}$ for $i \in A, j \in B$, then the neuronal activity in A and B is independent, i.e., a "patched" neuronal activity is observed in this case.

We stress here that certainly we could approximate the relationship as depicted in Fig. 4 more accurately, using for example a polynomial function. Nevertheless, as a first step to develop the MNN framework, we simply use Eq. (31) in the following.

In summary, from Eqs. (28), (30), and (31), we have the following relationship between inputs and outputs:

$$(\vec{\mu}^{(k+1)}, \vec{\sigma}^{(k+1)}, \rho^{(k+1)}) = \mathcal{M}(\vec{\mu}^{(k)}, \vec{\sigma}^{(k)}, \rho^{(k)}) \qquad (32)$$

where $\vec{\mu}^{(k)}=\{\mu_i^{(k)}, i=1,\ldots,p^{(k)}\}$, $\vec{\sigma}^{(k)}=\{\sigma_i^{(k)}, i=1,\ldots,p^{(k)}\}$ and $\mathcal{M}$ is the mapping defined by Eqs. (28), (30), and (31). Equation (32) gives us the relationship of the first- and the

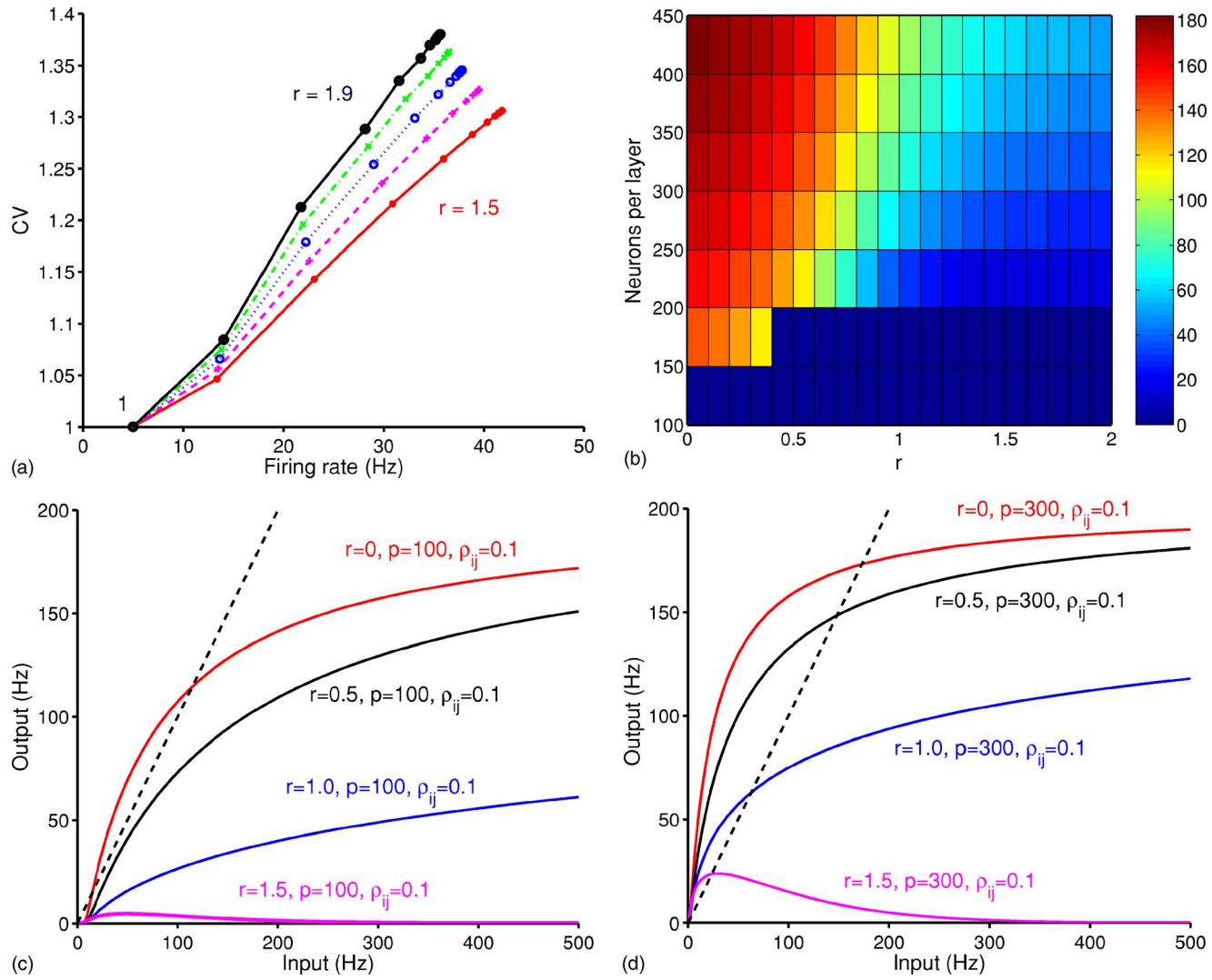

FIG. 6. (Color online) Propagation of activity in a homogeneous feedforward MNN. (Upper left) The mean output firing rate ($\mu_1^{(k)}$) and the coefficient of variation of the output interspike intervals ($C_1^{(k)}$) in the first 20 layers of the network, $k=1,\ldots,20$. Results obtained with $p^{(k)}=300$, $\mu_i^{(1)}=5$ Hz, $C_i^{(1)}=1$, $\rho_{ij}^{(k)}=0.1$, and $r=1.5,1.6,1.7,1.8,1.9$. Points labeled 1 correspond to the first layer; points corresponding to successive layers are connected by lines. (Upper right) Color intensity gives the mean firing rate (in Hz) observed in the 12th layer, as a function of the excitatory-inhibitory input ratio r and the number of neurons per layer. Results obtained for $\mu_i^{(1)}=10$ Hz,$C_i^{(1)}=1$. (Bottom left, right) The input-output firing rate relationships obtained for $p^{(k)}=100$ (left), 300 (right), and varying excitatory-inhibitory input ratio r. Note the appearance of a stable solution at low firing rate for networks of increasing size with strong inhibition.

second-order moments in a spiking neuronal network and is called moment mapping, which is one of the central results in the MNN. Note that the setup here is quite general and when $w_{jm}^{(k)}=0$ there is no connection between the jth and mth neurons.

IV. APPLICATIONS

The question we intend to address here is how a spontaneous activity can be maintained in a feedforward network. The parameters used for simulations are $V_{rest}=0$ mV, $L=1/20$ ms^{-1}, and $V_{th}=20$ mV, in agreement with most published results [36,7]. All simulations were carried out with MATLAB [37].

A. Spontaneous activity with clamped correlation

We start by considering a homogeneous network, where all weights, afferent means, and variances were set to be identical. Equation (32) then reduces to

$$(\vec{\mu}^{(k+1)},\vec{\sigma}^{(k+1)},\rho^{(k+1)})=\mathcal{M}(\vec{\mu}^{(k)},\vec{\sigma}^{(k)},\rho^{(k)}) \tag{33}$$

with $\mu_1^{(k)}=\mu_j^{(k)}$, $\sigma_1^{(k)}=\sigma_j^{(k)}$, $\rho_{12}^{(k)}=\rho_{mn}^{(k)}$, $m\neq n$. As we discussed before, the propagation of correlation becomes trivial in such case since all cells become fully correlated after the first layer. To avoid this, we "clamped" the correlation coefficient, i.e., we set $\rho_{ij}^{(k)}=\bar{\rho}$, $i\neq j$. In simulations we set $\bar{\rho}=0$ or 0.1, in agreement with experimental data reported in the literature [2,10]. Also, we set $p^{(k)}=100$, $w_{ij}=w=0.5$, and varied the ratio r in the range between 0 and 0.4.

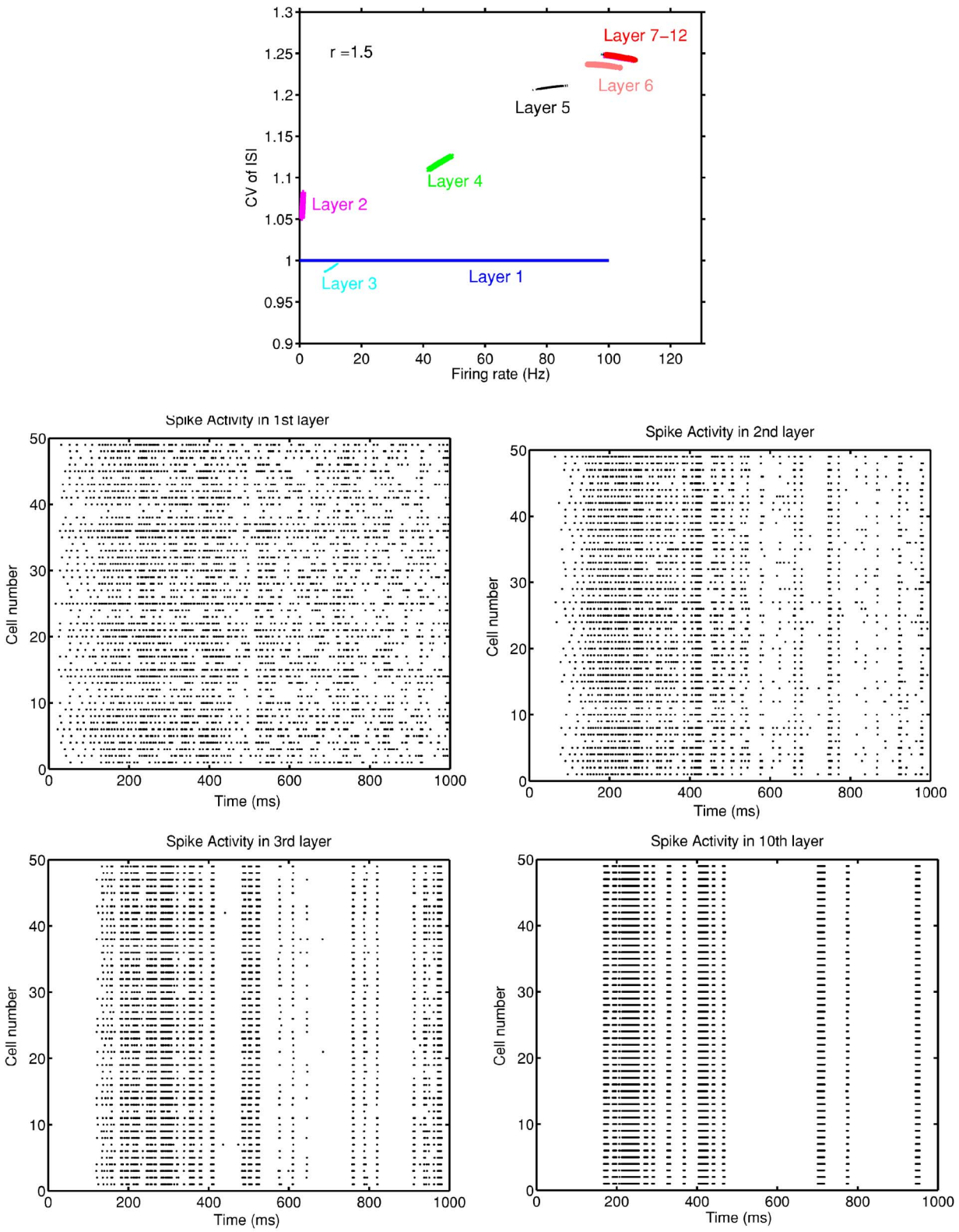

FIG. 7. (Color online) Propagation of activity in a feedforward MNN with random connections. (Top) The output CV vs the mean firing rate. (Middle, bottom) Raster plots of simulated activity in a feedforward spiking neuronal network (r=0.6), showing the progressive synchronization of neuronal activity through successive layers.

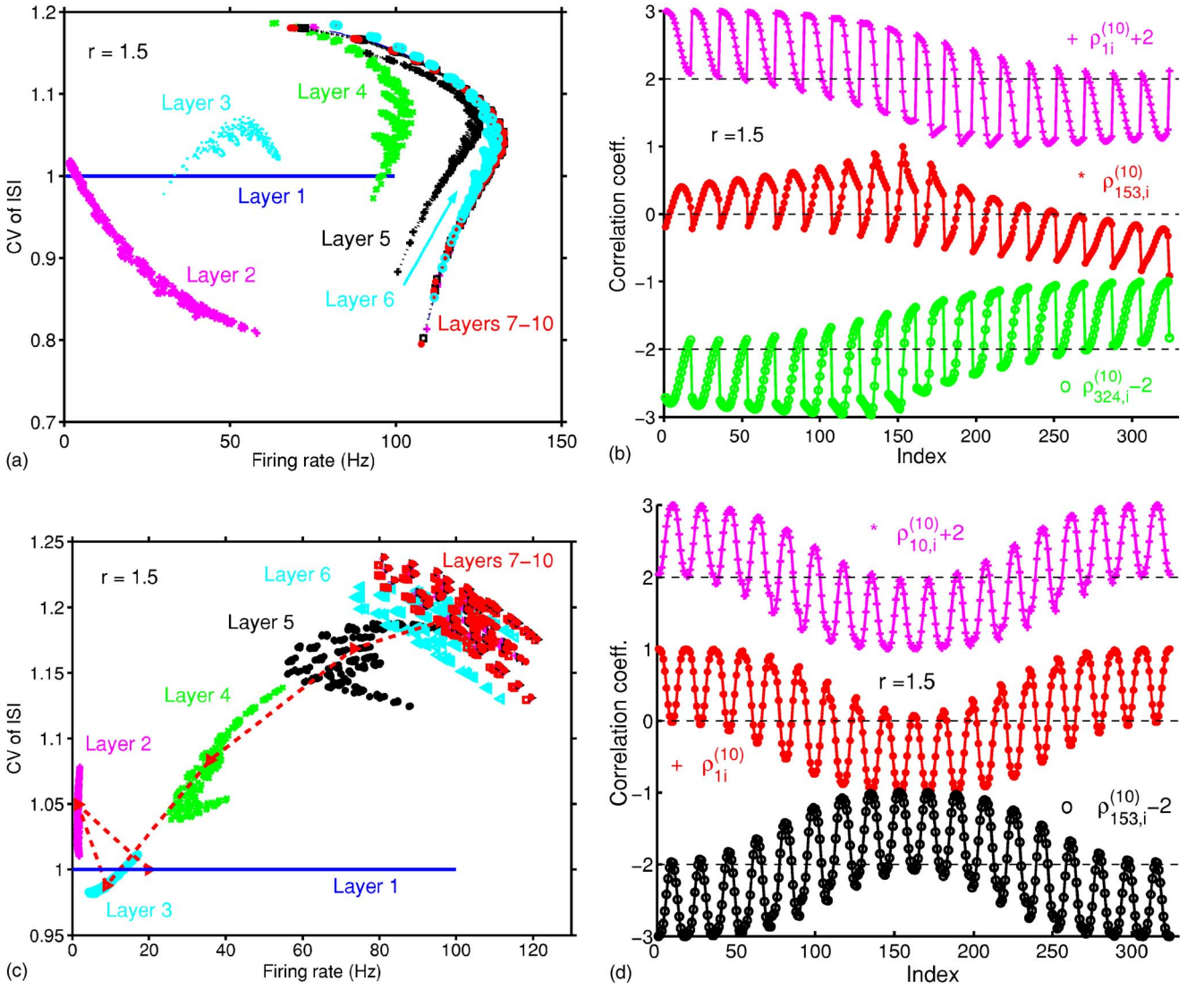

FIG. 8. (Color online) Propagation of activity in a feedforward MNN with Mexican hat type connections. (Top left) The output CV vs the mean firing rate in the first ten layers of the network (with open boundary conditions). (Top right) The correlation coefficients for three cells in layer 10. (Bottom) Same as above but with periodic boundary conditions. Parameters used for simulations: $r=1.5, p^{(k)}=324$, $k=1,2,\ldots,12, \rho_{ij}^{(1)}=0.1, \mu_i^{(1)} \sim U[0,100], C_i^{(1)}=1$.

In Fig. 5, we show the results obtained for various values of $\mu^{(1)}$ and $\sigma^{(1)}$ (we reported the coefficient of variation $C_i^{(k)}=\sigma_i^{(k)}/\mu_i^{(k)}$). Each data point $(\mu^{(k)}, C^{(k)})$ is connected with $(\mu^{(k+1)}, C^{(k+1)})$ to illustrate how the activity is propagated across the network. Figures 5 (top left, right; bottom right) show that after the first few layers, neurons are found to be either silent[2] or firing at relatively high frequency (about 100 Hz). We never found values of r between 0 and 1 that lead to a stable firing rate below 10 Hz. We also carried out a more detailed exploration of the network behavior in the range between $r=0.25$ and 0.3, with $\bar{\rho}=0.1$. The results shown in Fig. 5 confirm that the network activity converges to either high firing frequency or to silence.

Having observed this difficulty, we tried exploring a wider parameter region. From the results reported in Fig. 6 (upper panel left), we conclude that r must be significantly higher than 1 (exactly balanced input) for the network to display a stable activity at low firing rates. For instance, when $r=1.9$ and $\bar{\rho}=0.05$, the output firing rate was below 10 Hz, with a coefficient of variation of about 1.2 (data not shown). This also validates our approach since the output process is surely not a Poisson process, but a renewal process, i.e., $C_{\text{var}} \neq 1$.

The reason why such a high level of inhibition is necessary to maintain a spontaneous activity can be explained as follows. Depending on whether $0 \leqslant r \leqslant 1$ or $r > 1$, the input-output firing rate relationship of a neuron will be a sigmoidal or a skewed bell-shaped function [36], respectively. Since both functions start from the origin (see also Ref. [16], Fig. 8.13, middle panel), there will always be a fixed point of the

[2]We stop our simulation when the firing rate is slower than 0.001 Hz.

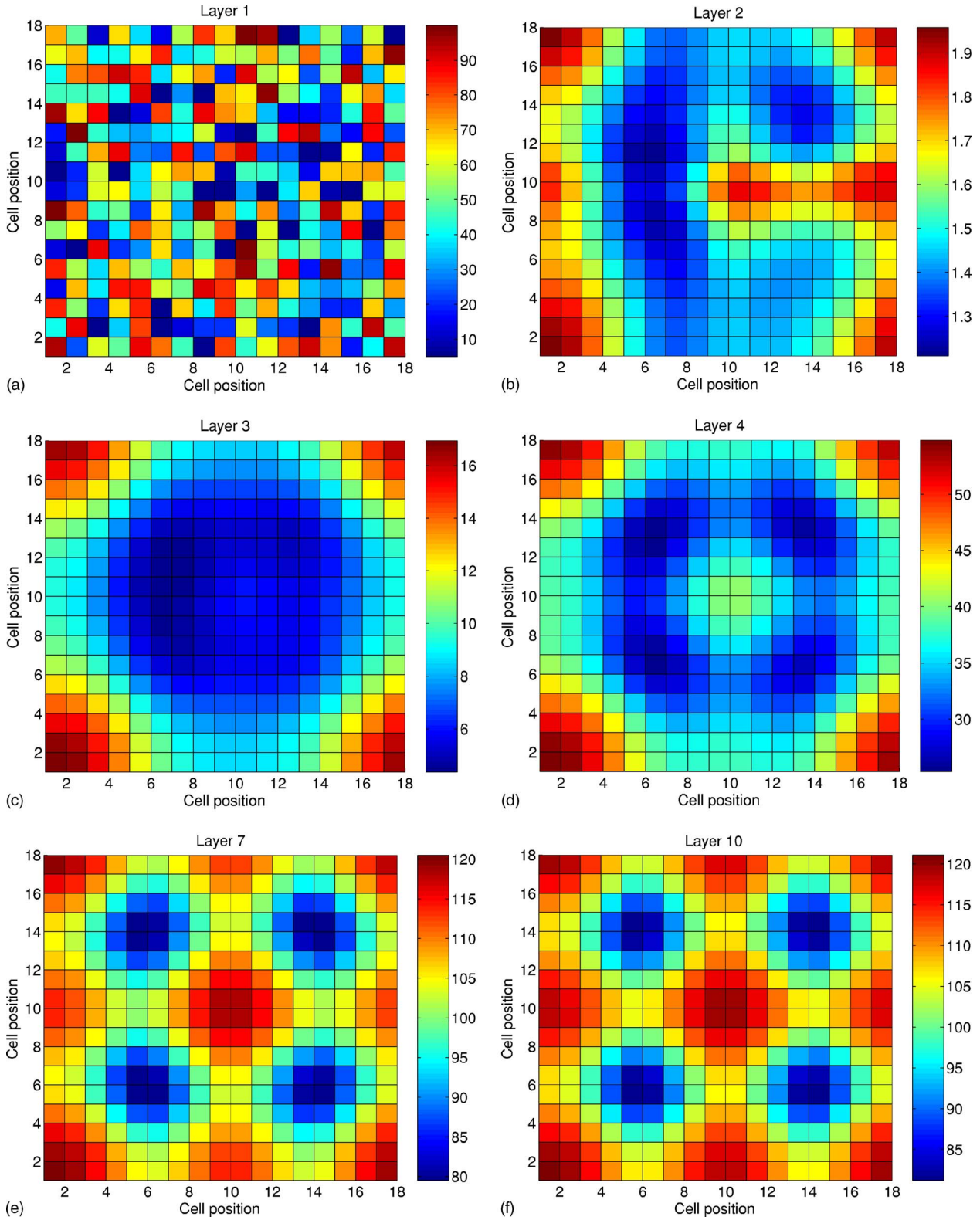

FIG. 9. (Color online) The mean firing rate for different layers, corresponding to Fig. 8 (bottom). Note the different scale for each layer.

system correspondent to the silence state. For a sigmoidal input-output function, there may be either one or three fixed points for the neuronal dynamics. In the latter case, both the silence state and the state at the highest firing rate are stable, and the system will settle on either one of the two depending on the input. However, for the existence of a fixed point at positive firing rate, a strong excitatory input is required, as shown in Fig. 6 (bottom), which also sets the stable firing rate at a relatively high level.

With a skewed-bell input-output function, instead, the fixed point at positive firing rate (whenever it exists) occurs at a significantly lower firing rate than for a sigmoid, see Fig. 6 (bottom right). Note that, for a skewed bell-shaped input-output function, there may be only two fixed points. In this case, the system may display a more complicated dynamics, with the appearance of limit cycles or chaotic activity.

We found that by increasing the number of neurons per layer we could obtain a larger encoding and decoding region for the system. For instance, when $p^{(k)}<200$ the output firing rate was either 0 or above 100 Hz, whereas for $p^{(k)}>250$ the output range was continuous. These conclusions remained true also when the threshold was set to $V_{th}=10$ mV [7] or a refractory period was included (data not shown).

In the literature, the assumption of exactly balanced spiking neuronal network is widespread (see for example Refs. [36,7,38]). However, with biologically reasonable parameters [7] we found that a feedforward spiking neuronal network cannot maintain a low-frequency spontaneous activity unless a *much* stronger inhibitory input is present. In this regard, it has recently been estimated in Ref. [32] that the magnitude of IPSP is about five times larger than that of EPSP, i.e., $b/a=5$ (see also Ref. [16], p. 239).

B. General case

We now turn to the case of a heterogeneous network and remove the constraint on the correlation coefficient between neurons. In accordance with the results reported in the previous subsection, we fixed the total number of neurons in each layer to $p^{(k)}=324$.

First we generated random connections $w_{ij}^{(k)}\in[0,0.5]$, and inputs $\mu_i^{(1)}\in[0,100]$ Hz. We also assumed that $(\sigma_i^{(1)})^2=\mu_i^{(1)}$ (i.e., the first layer is Poissonian), and that $\rho_{ij}^{(1)}=0.1$ for $i,j=1,\ldots,324$.

Simulations show that all neurons synchronize after the 4th layer, i.e., $\rho_{ij}^{(k)}=1$ for $k\geqslant 4$ and that the network is stable; see Fig. 7 (top). This result is in agreement with numerical experiments of feedforward spiking neuronal networks, showing that neurons get synchronized quite easily [17], as illustrated in Fig. 7 (middle and bottom panels). In fact, desynchronization rather than synchronization seems to be the major problem for a spiking neuronal network.

In order to avoid synchronization we introduced a Mexican hat weight distribution. To this end, we first rearranged all neurons $\{1,2,\ldots,p\}$ on a two-dimensional square lattice by assigning to neuron $i\in\{1,2,\ldots,p\}$ coordinates

$$x(i)=\left(\frac{i-1}{n}\right),$$

$$y(i)=(i-1)-nx(i)\equiv \mathrm{mod}(i-1,n) \tag{34}$$

with $p^{(k)}=n^2$. Then, for $i,j=1,2,\ldots,p^{(k)}$, and $k=1,2,\ldots$, we set

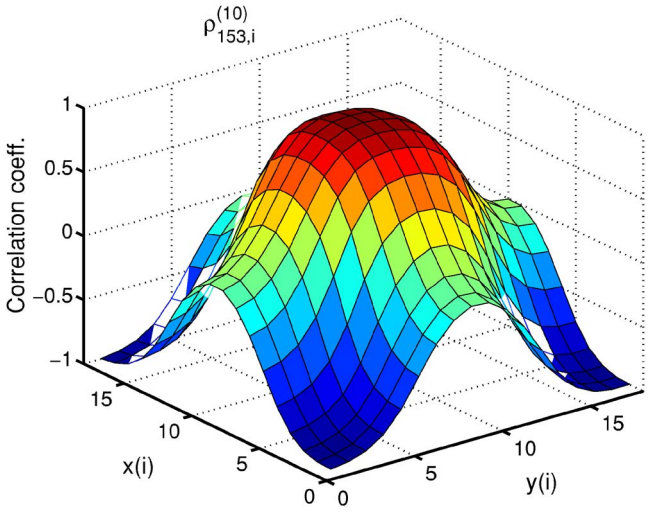

FIG. 10. (Color online) The correlations between the central cell in the tenth layer and the other cells in the same layer, corresponding to Fig. 8 (bottom).

$$w_{ij}^{(k)}=M(0.1[x(i)-x(j)],0.1[y(i)-y(j)]), \tag{35}$$

where $M(x,y)$ is the Mexican hat function, defined for $(x,y)\in\mathbf{R}^2$ as

$$M(x,y)=\frac{m}{\sqrt{2\pi\gamma}}\left[\exp\left(-\frac{x^2+y^2}{2\gamma^2}\right)-\frac{1}{2}\exp\left(-\frac{x^2+y^2}{8\gamma^2}\right)\right] \tag{36}$$

with $m>0$, $\gamma>0$ modulation parameters. For simulations we used $m=3$, $\gamma=0.5$. Also we set $\mu_i^{(1)}\in U[0,100]$ Hz, $(\sigma_i^{(1)})^2=\mu_i^{(1)}$, and $\rho_{ij}^{(1)}=0.1$.

The results shown in Fig. 8 indicate that the activity in the network becomes stable after the sixth layer. Also, as indicated by the values of the correlation coefficients (right panel), the neurons do not synchronize, and the mean correlation coefficient between neurons was around zero. In other words, the lateral inhibition introduced by the Mexican hat pushes cells to fire with more widely spread firing rates than in a network with random interactions.

To avoid boundary effects due to the finite size of the system, we rerun simulation using periodic boundary conditions. The results are shown in Fig. 8 (bottom panel) (see Fig. 9 for more details). In Fig. 10 we plotted the correlations for the central cell in the tenth layer: on average the correlation coefficient is slightly negative, in agreement with experimental observations [39,40]. Figure 11 shows the results obtained with $r=1.1$.

It is interesting to note that from the first to the second layer, there is a general reduction in firing rate. Then, after a few transition layers, the neuronal activity becomes stable, with firing rates distributed around 100 Hz and a CV greater than 0.5. In summary, the activity in a MNN becomes stationary after a few layers. With random interactions, the network gets easily synchronized. However, with lateral interactions, firing rates of individual neurons tend to spread out.

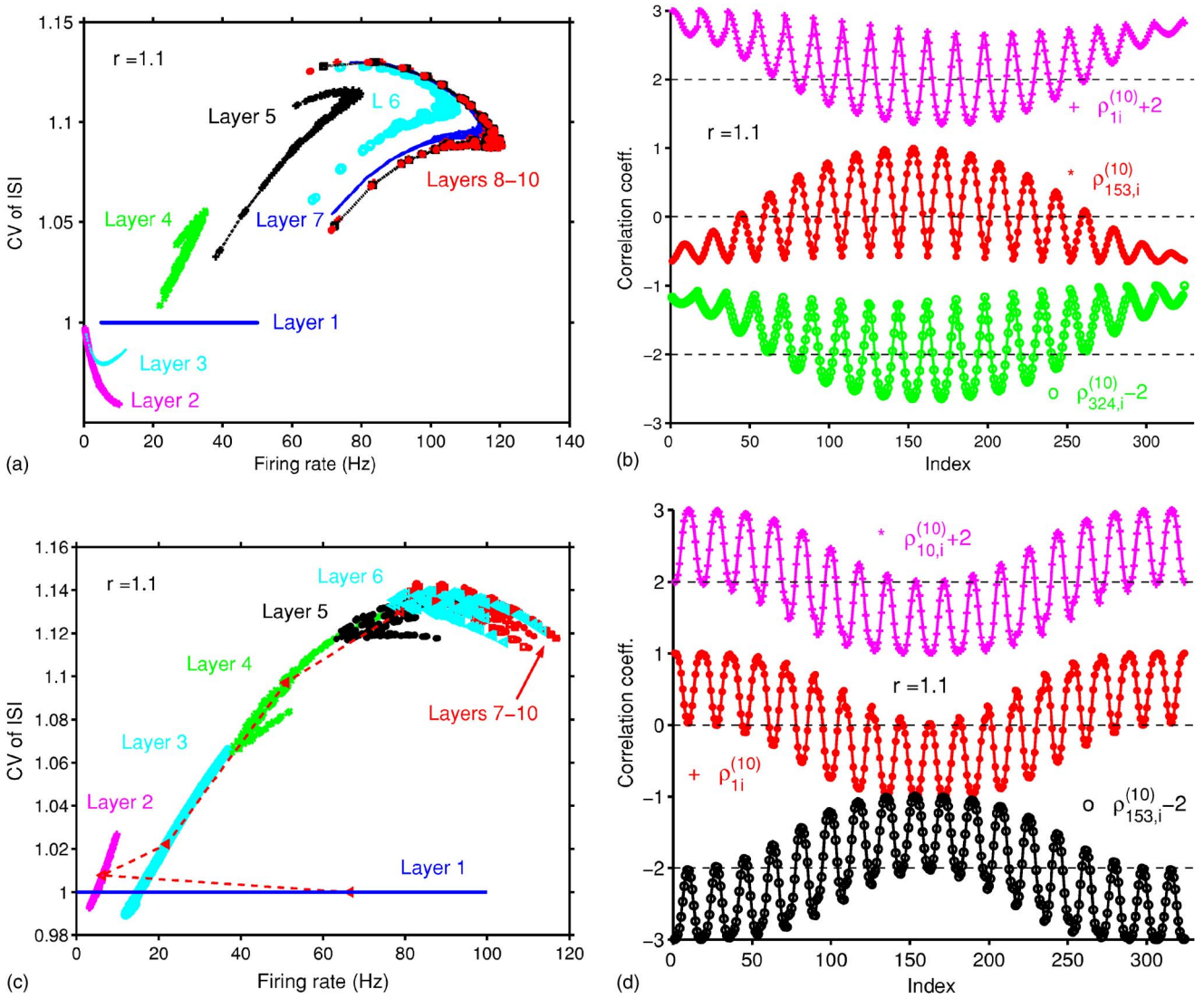

FIG. 11. (Color online) Propagation of activity in a feedforward MNN with mexican hat type connections. (Top left) The output CV vs the mean firing rate in the first ten layers of the network (with open boundary conditions). (Top right) The correlation coefficients for three cells in layer 10. (Bottom) Same as above but with periodic boundary conditions. Parameters for simulations were as in Fig. 8, but $r=1.1$.

Finally, the network simulations reported here show that an highly irregular output firing is produced as a result of correlations between neuronal activity [41–43]. This confirms our general findings [2] that correlated input is key to generate irregular spike trains (say, with $C_{\mathrm{var}}>0.5$).

V. DISCUSSION

To approximate neuronal models with renewal process inputs has always been a bottleneck for the development of a theory of spiking neuronal networks, since even the simplest neuronal model, the integrate-and-fire model, emits spike trains which are renewal processes. In this paper, we have presented two schemes, the UAS and the OUS, that serve this purpose. Using numerical simulations, we have demonstrated that both schemes work well for the integrate-and-fire model.

Based upon these results, we have developed a framework of moment neuronal networks, where the network behavior depends on both the mean and the fluctuations and correlations of spike activity. Within this context, we have considered how spontaneous activity can be maintained in a feedforward spiking neuronal network. Our results suggest that a necessary condition is that the inhibitory input be muchstronger than the excitatory input. Whether such strong inhibition is present also during periods of stimulated activity is an open problem. If the nervous system does reduce the inhibitory input during such periods, it is natural to ask to what extent and how this reduction is achieved.

In the current paper we have focused on the case of stationary interactions. In the near future, we intend to generalize our framework to the nonstationary case and introduce a suitable mechanism for learning, based on the ideas developed in the ANN. This might, for instance, shed light on how the inhibitory input changes during different periods of activation.

The results presented here should be considered as an attempt toward a theory of computation with stochastic sys-

tems. Under this respect, the MNN framework plays the role of the central limit theorem in the probability theory, whereas earlier approaches, based exclusively upon the mean, could be likened to the law of large numbers.

VI. ACKNOWLEDGMENT

J. Feng was partially supported by UK EP/C51338X/, EP/D051916/, and GR/S30443/01.

[1] L. F. Abbott and P. Dayan, Neural Comput. **11**, 91 (1999).
[2] J. F. Feng and D. Brown, Neural Comput. **12**, 671 (2000).
[3] B. W. Knight, J. Gen. Physiol. **59**, 734 (1972).
[4] B. W. Knight, J. Gen. Physiol. **59**, 767 (1972).
[5] F. Liu, J. F. Feng, and W. Wang, Europhys. Lett. **64**, 131 (2003).
[6] E. Salinas and T. J. Sejnowski, Nat. Rev. Neurosci. **2**, 539 (2001).
[7] M. N. Shadlen and W. T. Newsome, Curr. Opin. Neurobiol. **4**, 569 (1994).
[8] H. Sompolinsky *et al.*, Phys. Rev. E **64**, 051904 (2001).
[9] C. F. Stevens and A. M. Zador, Nat. Neurosci. **1**, 210 (1998).
[10] E. Zohary, M. N. Shadlen, and W. T. Newsome, Nature (London) **370**, 140 (1994).
[11] L. F. Abbott, J. A. Varela, K. Sen, and S. B. Nelson, Science **275**, 220 (1997).
[12] D. J. Amit and N. Brunel, Network Comput. Neural Syst. **8**, 373 (1997).
[13] N. Brunel, J. Comput. Neurosci. **8**, 183 (2000).
[14] N. Brunel and V. Hakim, Neural Comput. **11**, 1621 (1999).
[15] J. F. Feng, *Computational Neuroscience—A Comprehensive Approach* (Chapman & Hall/CRC Press, Boca Raton, 2003).
[16] W. Gerstner and W. Kistler, *Spiking Neuron Models* (Cambridge University Press, Cambridge U.K., 2003).
[17] H. C. Tuckwell, *Introduction to Theoretical Neurobiology* (Cambridge University Press, Cambridge, U. K., 1988), Vol. 2.
[18] A. L. Fairhall *et al.*, Nature (London) **412**, 787 (2002).
[19] N. Fourcaud and N. Brunel, Neural Comput. **14**, 2057 (2002).
[20] M. S. Goldman, P. Maldonado, and L. F. Abbott, J. Neurosci. **22**, 584 (2002).
[21] G. Leng *et al.*, J. Neurosci. **21**, 6967 (2001).
[22] A. Longtin, F. Moss, and A. Bulsara, Phys. Rev. Lett. **67**, 656 (1991).
[23] M. Mattia and P. Del Giudice, Phys. Rev. E **66**, 051917 (2002).
[24] D. Q. Nykamp and D. Tranchina, J. Comput. Neurosci. **8**, 19 (2000).
[25] F. Rieke, D. Warland, R. de Ruyter van Steveninck, and W. Bialek, *Spikes* (MIT Press, Cambridge, MA, 1997).
[26] A. Treves, Networks **4**, 259 (1993).
[27] X. J. Wang, J. Neurosci. **19**, 9587 (1999).
[28] D. Aldous, *Probability Approximations via the Poisson Clumping Heuristic*, Applied Mathematical Sciences Ser. Vol. 77 (Springer-Verlag, New York, 1989).
[29] W. Feller, *An Introduction to Probability Theory and its Applications*, 3rd ed. (Wiley, New York, 1960), Vol. 2.
[30] J. J. Humter, Adv. Appl. Probab. **6**, 546 (1974).
[31] L. M. Ricciardi and S. Sato, in *Lectures in Applied Mathematics and Informatics*, edited by L. M. Ricciardi (Manchester University Press, Manchester, 1990).
[32] L. F. Abbott and C. van Vreeswijk, Phys. Rev. E **48**, 1483 (1993).
[33] P. R. Cox and P. A. W. Lewis, *The Statistical Analysis of Series of Events* (Latimer Trend & Co., Whitstable, 1966).
[34] D. Brown, J. F. Feng, and S. Feerick, Phys. Rev. Lett. **82**, 4731 (1999).
[35] J. F. Feng and G. Li, J. Phys. A **34**, 1649 (2001).
[36] V. Livak, H. Sompolinsky, I. Segev, and M. Abeles, J. Neurosci. **23**, 3006 (2003).
[37] The programs are available at http://www.cogs.susx.ac.uk/users/jianfeng/publications. We are thankful to Nicolas Brunel for providing us with part of the MATLAB code.
[38] C. van Vreeswijk and H. Sompolinsky, Science **274**, 1724 (1996).
[39] A. U. Nicol, M. S. Magnusson, A. Segonds-Pichon, A. Tate, J. Feng, and K. M. Kendrick (unpublished).
[40] A. J. Tate, A. U. Nicol, H. Fischer, A. Segonds-Pichon, J. Feng, M. S. Magnusson, and K. M. Kendrick (unpublished).
[41] N. Brunel, Networks **11**, 261 (2000).
[42] N. Brunel, F. Chance, N. Fourcaud, and L. F. Abbott, Phys. Rev. Lett. **86**, 2186 (2001).
[43] J. F. Feng and H. C. Tuckwell (unpublished).